The Astrophysical Journal, 617:171–183, 2004 December 10

AVERAGE ULTRAVIOLET QUASAR SPECTRA IN THE CONTEXT OF EIGENVECTOR 1: A BALDWIN EFFECT GOVERNED BY THE EDDINGTON RATIO?

R. Bachev,[1,2] P. Marziani,[3] J. W. Sulentic,[1] R. Zamanov,[4] M. Calvani,[3] and D. Dultzin-Hacyan[5]

Received 2004 March 2; accepted 2004 August 18

ABSTRACT

We present composite UV spectra for low-redshift type 1 active galactic nuclei binned to exploit the information content of the eigenvector 1 (E1) parameter space. Composite spectra show high enough S/N and spectral resolution to permit a decomposition of the C IV λ1549 line profile: one of the strongest high-ionization lines (HILs), and fundamental in defining E1 space. The simplest C IV λ1549 decomposition into narrow-line region (NLR), broad-line region (BLR), and very broad line region (VBLR) components suggests that different components have an analog in Hβ with two major exceptions. VBLR emission is seen *only* in population B [FWHM(H$\beta_{\rm BC}$) $>$ 4000 km s^{-1}] sources. A blueshifted/asymmetric BLR component is seen *only* in population A [FWHM(H$\beta_{\rm BC}$) $\leq$ 4000 km s^{-1}] HILs such as C IV λ1549. The blueshifted component is thought to arise in a high-ionization wind or outflow. Our analysis suggests that such a wind can only be produced in population A (almost all radio-quiet, RQ) sources, where the accretion rate is relatively high. We propose a model to account for several differences between low- and high-ionization line profiles. Part of the broad-line emission is attributed to a self-gravitating/fragmented region in an accretion disk. An inner, optically thick, geometrically thin region of the flow may give rise to a wind/outflow and produce the blueshifted HIL spectrum in population A sources. The fragmented region may produce all or most of the broad-line emission in population B, which contains RQ and the majority of radio-loud (RL) quasars. Comparison between *broad* UV lines in RL and RQ sources in a single, well-populated E1 parameter space bin (B1) shows few significant differences. Clear evidence is found for a significant NLR C IV component in most RL sources. The BLR/VBLR similarity in bin B1 provides circumstantial evidence in favor of black hole (BH) spin, rather than BH mass or accretion rate, as a key trigger in determining whether an object will be RL or RQ. We find a 10-fold decrease in EW C IV λ1549 with Eddington ratio (decreasing from $\approx$1 to $\sim$0.01), while N V λ1240 shows no change. These trends suggest a luminosity-independent "Baldwin effect" in which the physical driver may be the Eddington ratio.

Subject headings: methods: statistical — quasars: emission lines — quasars: general

1. INTRODUCTION

Understanding the geometry and kinematics of the central regions in active galactic nuclei (AGNs) is one of the major goals of 21st century astronomy. Yet little is known beyond the necessity of invoking accretion onto a supermassive object in order to account for the enormous source luminosity. Given our inability to resolve the central regions of even the nearest AGNs, we are left with three approaches toward achieving our goal. These are (1) ideology: sophisticated models driven entirely by theories describing black hole and associated accretion disk properties (e.g., Janiuk et al. 2000; Gammie et al. 2004); (2) analogy: comparison with better resolved galactic objects (e.g., interacting binary stars; Zamanov & Marziani 2002; Mirabel 2004; Maccarone et al. 2003); and (3) empiricism: detailed studies of phenomenology in large and diverse samples of AGNs (see Sulentic et al. 2000a for references until late 1999; Marziani et al. 2003a, hereafter M03; Dietrich et al. 2002; Kuraszkiewicz et al. 2004 for examples of more recent works). The last approach fell on hard times until the end of the 20th century, in part because of (1) the apparent intractability of AGN phenomenology, (2) the failure of the best nebular physics models to reproduce the observed spectra, and (3) the low quality of so much of the spectroscopic data. Thus we now know more about the morphology of the extended radio and optical emission around quasars than the underlying geometry/physics that drives them. One positive development involves the application of reverberation mapping toward estimation of the broad-line region size (see Peterson 1993 for a thorough review; see Horne et al. 2004 for up-to-date expectations). The relevant questions are how to interpret these data and, more importantly, how to select a representative sample of sources for a reverberation mapping study. Another positive development involves growing databases of AGN spectra (most notably from the Sloan Digital Sky Survey [SDSS]; Richards et al. 2002; Schneider et al. 2002). Although a great part of the individual data still suffers from S/N limitations, average or composite spectra of many objects can significantly improve the situation (Vanden Berk et al. 2001; Sulentic et al. 2002). One of the most important questions is *how* to bin the data. Clearly, unrestricted composites have little value because they hide the intrinsic dispersion in key parameters that provides clues to the underlying physics (e.g., Francis et al. 1991). In a previous paper (Sulentic et al. 2002, hereafter Paper I), we argue that composite spectra binned within the eigenvector 1 (E1) parameter space provide the most physically useful results. Paper I presented composites of the Hβ spectral region, and this paper presents complementary composites for the UV spectral region and especially for C IV λ1549.

[1] Department of Physics and Astronomy, University of Alabama, Tuscaloosa, AL 35487; giacomo@merlot.astr.ua.edu.
[2] Institute of Astronomy, Sofia 1784, Bulgaria; bachevr@astro.bas.bg.
[3] INAF–Osservatorio Astronomico di Padova, Vicolo dell'Osservatorio 5, I-35122 Padova, Italy; marziani@pd.astro.it, calvani@pd.astro.it.
[4] Astrophysics Research Institute, Liverpool John Moores University, Twelve Quays House, Birkenhead, CH41 1LD, UK.
[5] Instituto de Astronomía, UNAM, Apartado Postal 70-264, 04510 Mexico DF, Mexico; deborah@astroscu.unam.mx.

We have identified a four-dimensional parameter space that overcomes some of the problems mentioned above and that offers a new perspective on AGN phenomenology (Sulentic et al. 2000a, 2000c). The E1 parameter space provides optimal discrimination/unification of broad-line AGN classes (Boroson & Green 1992; Marziani et al. 2001, hereafter M01; Boroson 2002). The adopted name reflects recognition of the first two parameters in the pioneering work of Boroson & Green (1992). E1 as we now define it involves measures of the following:

1. FWHM of low-ionization (LIL) broad emission lines [FWHM($H\beta_{BC}$)];
2. equivalent width (EW) ratio of optical Fe II and $H\beta_{BC}$: $R_{Fe\,II}$ = EW(Fe II λ4570 blend)/EW($H\beta_{BC}$);
3. soft X-ray photon index (Γ_{soft}); and
4. profile centroid velocity displacement (at FWHM) for C IV λ1549.

In the simplest terms these parameters can be said to measure, respectively, (1) velocity dispersion of LIL-emitting gas, (2) relative strength of LIL features thought to arise in the same region, (3) strength of a soft X-ray component, and (4) amplitude of systematic motions in the high-ionization line (HIL) emitting gas. In less simple (i.e., more model-dependent) terms, we likely have (1) two variables mainly sensitive to accretion rate [FWHM($H\beta_{BC}$) and Γ_S: Nicastro 2000; M01; Pounds et al. 1995; Czerny et al. 2004] and (2) three variables sensitive to source orientation (all with the possible exclusion of Γ_S; e.g., Jackson & Browne 1991; Wills et al. 1995; Marziani et al. 1996; M01; Rokaki et al. 2003; Sulentic et al. 2003); $R_{Fe\,II}$ is sensitive to nebular physics (electron density n_e and column density N_c).

An important addition that reflects the striking changes in emission-line properties across E1 involves the introduction of the population A and B concept. At present, we arbitrarily define population A and B quasars as those with FWHM $H\beta_{BC}$ less than or greater than 4000 km s^{-1}. It is unclear whether the A-B concept reflects two distinct quasar populations or simply the difference in mean properties of sources at opposite ends of the E1 "main sequence." The "elbow" shape of the sequence, and optical/X-ray indications (Sulentic et al. 2000a, 2000c; Komossa & Meerschweinchen 2000) for a "zone of avoidance" near FWHM($H\beta_{BC}$) $\approx$ 4000 km s^{-1}, provide some evidence in support of the former interpretation. If the distinction is real, then "A" is a largely radio-quiet (RQ) population (including narrow-line Seyfert 1 sources as an extremum), while "B" contains a mix of broader line RQ plus most radio-loud (RL) sources. The population A-B distinction will prove useful in this study, and C IV λ1549 will add support for the concept (§§ 3.2 and 4.3).

If the E1 concept lives up to its initial promise, it may be the strongest and most encompassing type 1 AGN unification yet discovered. This possibility warrants strong tests of its strength and generality. So far, most of our effort has centered on the "optical plane" of E1 (M01; Zamanov et al. 2002; Boroson 2002; Marziani et al. 2003a, 2003b; Sulentic et al. 2003). This focus has been dictated by the available X-ray and UV archival data that provide the other E1 parameters. In § 2 we present composite spectra for C IV λ1549 (and other UV lines) in the E1 context, which complements the work already done for $H\beta$.

2. GENERATING COMPOSITE UV SPECTRA

A total of about 700 reasonable quality (S/N $\geq$ 4–5)[6] *Hubble Space Telescope* (*HST*) spectra for $n = 141$ different AGNs (quasars or bright Seyfert 1 galaxies; $n = 61$ are RL with $R_K \gtrsim 100$, where R_K is the specific flux ratio between 4400 Å and 6 cm) have been extracted from the Hubble archive. The majority of the spectra (83%) were obtained with the FOS camera, and the rest with STIS. The FOS/BL data (40%) were recalibrated with the latest IRAF package STPOA, which takes into account some systematic errors in the wavelength calibration. No such recalibration is available for the FOS/RD, where similar errors are known to exist, which ultimately limits the wavelength accuracy of our composites to about 0.5–1.0 Å (see, for instance, Kerber & Rosa 2000 for details on FOS calibration).

Composite spectra cover the entire rest-frame region between 1000–3000 Å, while individual source spectra will often cover only a part of it. We applied the following procedures to compute the composite spectra:

1. Spectra for a specific source covering the same spectral region were averaged together (if they were of comparable S/N).
2. A single spectrum for each object was created by adding the parts covering different wavelength regions, with slight adjustments of the continuum levels if necessary.
3. All spectra were corrected for Galactic extinction following Schlegel et al. (1998). The typical extinction correction A_V was about 0.1–0.2 mag. No correction for the intrinsic extinction was attempted.
4. The spectra were deredshifted using the most accurate available measurements (M03) or by using the latest accurate values available in the literature whenever a source was not part of the M03 sample.[7] It should be noted that redshifts from Véron-Cetty & Véron (2001, hereafter VCV01) sometimes differ considerably from our best values (Δz could be as large as 0.02).
5. Spectra were normalized by their own continuum flux in the wavelength range 1430–1470 Å, where no strong lines are observed/expected.
6. Composite spectra were generated by median-combining the averaged spectra of individual AGNs. This procedure ensures that only the most typical features will be revealed and that some unusual features, such as narrow absorption (often lost in the noise), unusually strong (narrow) lines, and noise spikes, will be omitted in the composites. A median also works better than an average when the individual spectra do not cover the same spectral region (see § 4 for details regarding line profiles of the composites).

The composites have been binned to 0.5 Å per resolution element and have a typical S/N $\sim$ 50 (see Table 1). The composite spectra are presented in Figure 1 with an enlargement of the 1100–2000 Å region of greatest interest shown in Figure 2. The latter show details of the strongest lines such as Lyα, C IV λ1549, and C III] λ1909. The lines that we identified and measured (§ 3.1) are labeled.

We defined spectral types on the basis of source parameter properties in the optical plane of E1 (Paper I). This approach differs from the one employed in analysis of the SDSS quasar sample (Richards et al. 2002), where sources were binned a posteriori in terms of the velocity shift between C IV λ1549 and Mg II λ2800. We are able to create useful composites for five

[6] Here and below, S/N is the signal-to-noise ratio per resolution element, measured in the continuum, blueward of C IV λ1549.

[7] M03 did not publish most of their refined redshift measures based on [O III] λ5007 or the narrow peak of $H\beta$ (see Zamanov et al. 2002); they are available from the authors on request.

TABLE 1
DEFINITION OF SPECTRAL TYPES

Bin (1)	FWHM($H\beta_{BC}$) (2)	$R_{Fe\,II}$ (3)	$N_{tot}(N_{RL})$ (4)	S/N (5)	$\langle M_V \rangle$ (σ) (6)	$\langle z \rangle$ (σ) (7)	EW([O III]) (8)	EW($H\beta$) (9)
A3.....	<4000	>1.0	10 (2)	39	−23.1 (2.1)	0.20 (0.20)	20 (5)[a]	50 (54)
A2.....	<4000	0.5–1.0	14 (1)	35	−24.4 (1.6)	0.26 (0.22)	18 (9)	67 (63)
A1.....	<4000	<0.5	40 (12)	74	−24.3 (2.2)	0.26 (0.24)	44 (25)	95 (89)
B1.....	4000–8000	<0.5	54 (28)	87	−25.1 (1.7)	0.36 (0.24)	46 (26)	98 (95)
B1+.....	>8000	<0.5	21 (17)	52	−25.4 (1.4)	0.44 (0.22)	60 (34)	99 (98)

NOTES.—Col. (1): Spectral type designation following Paper I. Col. (2): Range of FWHM($H\beta_{BC}$). Col. (3): Range of $R_{Fe\,II}$. Col. (4): Number of sources used for the composite spectrum (number of RL source in parentheses). Col. (5): Each bin typically involves 15–30 sources resulting in a S/N in the continuum of typically 40–60. Cols. (6) and (7): Average absolute V magnitude (computed from VCV01; $H_0 = 50$ km s^{-1} Mpc^{-1}; $q_0 = 0$ is adopted) and redshift for sources used in the bin composite followed by the sample standard deviations. Cols. (8) and (9): Average EWs of [O III] λ5007 and $H\beta$, respectively, for the objects of the sample.

[a] We provide the median values (in parentheses) for Cols. (8) and (9) as well. Because of significantly dispersed EW distributions and the small number of objects in some bins, the medians may differ significantly from the averages, especially for [O III].

E1 bins with fixed FWHM($H\beta_{BC}$) and $R_{Fe\,II}$ ranges, exactly as done in Paper I. The values of FWHM($H\beta_{BC}$) and $R_{Fe\,II}$ that provide an optical bin assignment were taken from M03. In order to maximize the number of sources in each bin, we also include additional spectra for sources (≈20% of the total), not part of the M03 sample. This supplemental data involves (1) sources with reasonable quality archival C IV λ1549 data and (2) $H\beta$ spectra from literature sources with high enough S/N to permit assignment into one of the predefined E1 bins. Details on bin assignation for individual sources that are not part of the M03 sample will be provided in a future work. Table 1 provides parameter measures and statistical properties for the spectral bins.

There is a clear trend between $\langle M_V \rangle$ and z, in the sense that population A sources show lower mean redshift and luminosity. This is a known bias in the M03 data set. M03 is a step toward our goal to develop a sample complete to $m_V = 16.5$. At this time, the RL part of our sample is apparently complete (the standard V/V_{max} completeness test, e.g., Peterson 1997, gives ∼0.8 compared to 0.3 for RQ sources). The RL sources tend to be more luminous (due in part to relativistic beaming), resulting in selecting more high-redshift sources. The E1 optical parameters *show no dependence on luminosity* to at least $z \lesssim 1$ and $m_V \lesssim 16.5$ (Sulentic et al. 2004). We will consider later possible UV line versus source luminosity correlations (see §§ 3.3 and 4.3).

We also computed the sample standard deviation for the spectra in each bin. Deviations from the composites at 1 σ confidence level are found to be about 20% and show no specific features after being normalized by the composites themselves.

3. UV LINES IN THE E1 CONTEXT

3.1. Fe II$_{UV}$ *Subtraction and Line Measurements*

Table 2 presents rest-frame EW and FWHM measures for UV lines in the composite spectra. E1 bin designations are

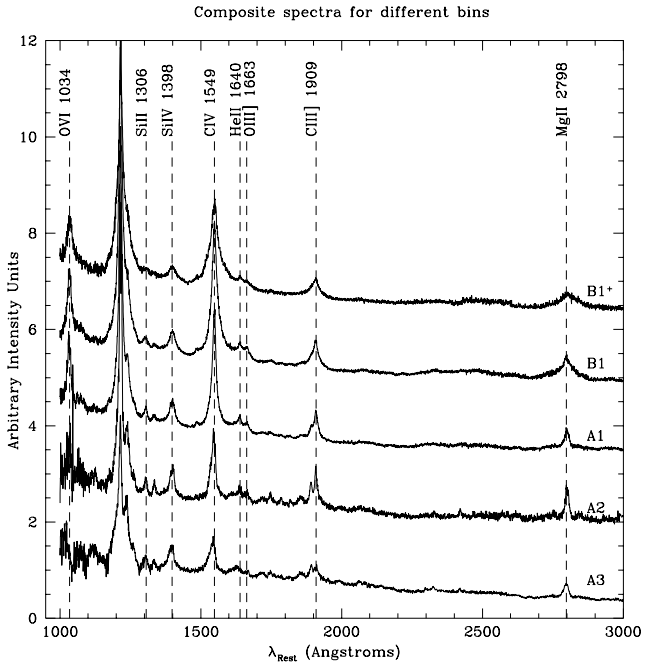

FIG. 1.—Median *HST* spectra for the five spectral types considered in this paper, with identification of the strongest emission lines. Each spectrum was corrected for the interstellar extinction and shifted to the rest frame before being processed. Horizontal scale is rest frame wavelength in Å; vertical scale is in arbitrary F_λ intensity units. Spectra have been offset on the vertical axis for clarity.

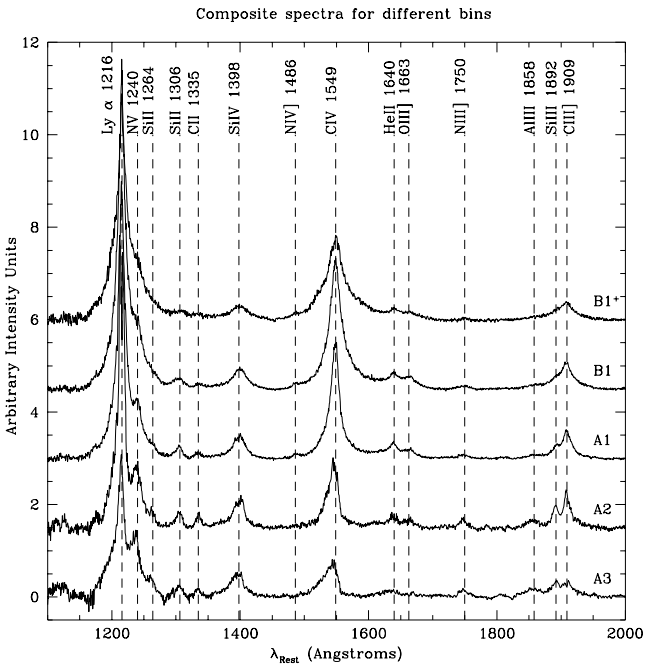

FIG. 2.—Rest-frame region of the median spectra between 1150 and 1950 Å is shown after continuum and Fe II$_{UV}$ emission subtraction. As for Fig. 1, spectra have been offset for clarity. All lines for which we report EW and FWHM in Table 2 are identified. Horizontal scale is rest-frame wavelength in Å.

TABLE 2
LINE MEASUREMENTS

	A3		A2		A1		B1		B1$^+$	
LINE ID	EW (σ)	FWHM (σ)	EW (σ)	FWHM (σ)	EW (σ)	FWHM (σ)	EW (σ)	FWHM (σ)	EW (σ)	FWHM (σ)
O VI 1034	...	...	...	...	17 (4)	3770 (500)	21 (6)	4350 (600)	18 (4)	5510 (700)
C III 1176	...	...	4 (3)	3600 (2000)	1 (1)	5100 (2000)	4 (3)	5350 (2500)	...	...
Lyα 1216	48 (15)	2960 (700)	92 (21)	2960 (500)	101(25)	3450 (500)	116(21)	3700 (400)	93 (18)	5420 (400)
N V 1240	26 (9)	3870 (700)	21 (7)	4110 (700)	17 (6)	3380 (600)	28 (9)	5080 (800)	25 (6)	7250 (900)
Si II 1264	3 (2)	2250 (1000)	2 (1)	1420 (800)	...	...	...	...	...	...
Si II 1306	6 (2)	3530 (500)	5 (1)	2290 (300)	3 (1)	2290 (300)	4 (1)	3670 (500)	3 (1)	4820 (1000)
C II 1335	2 (1)	1970 (500)	3 (1)	1680 (300)	1 (1)	2240 (300)	1 (1)	2240 (600)	1 (1)	3590 (1500)
Si IV 1398	16 (3)	4500 (400)	16 (3)	3860 (400)	13 (3)	4070 (400)	11 (2)	3640 (400)	12 (2)	6000 (400)
N IV] 1486	...	...	...	...	2 (1)	2610 (800)	1 (1)	3020 (800)	...	...
C IV 1549	23 (4)	4160 (400)	35 (9)	3290 (400)	69 (16)	3480 (400)	83 (16)	4260 (400)	79 (10)	6190 (400)
He II 1640	8 (2)	5850 (700)	10 (2)	4750 (500)	11 (2)	4570 (400)	11 (2)	4930 (500)	4 (1)	4750 (600)
O III] 1663	2 (1)	2880 (800)	5 (2)	4140 (700)	4 (1)	3060 (500)	7 (2)	4320 (700)	5 (2)	3600 (700)
N III] 1750	4 (3)	2050 (1000)	...	...	...	...	4 (3)	4410 (1500)	...	...
Al III 1860	8 (4)	4670 (1200)	5 (3)	3860 (1200)	2 (1)	4180 (1000)	3 (2)	4700 (2000)	3 (2)	5700 (2500)
Si III] 1892	7 (3)	1900 (800)	8 (2)	1740 (700)	6 (2)	2530 (600)	5 (3)	2530 (1000)	3 (2)	3010 (1500)
C III] 1909	10 (4)	2350 (800)	15 (4)	1720 (700)	17 (4)	2510 (500)	20 (7)	3140 (700)	18 (9)	3920 (1200)
Mg II 2798	12 (8)	2030 (700)	14 (4)	1500 (700)	16 (2)	1600 (600)	40 (8)	3960 (600)	44 (8)	6540 (600)
Fe II$_{UV}$	22 (10)	3000 (...)	16 (8)	3000 (...)	9 (5)	3000 (...)	7 (5)	5000 (...)	7 (5)	9000 (-)

listed at the top of the table. Uncertainty estimates are given in parentheses following each measure. EW uncertainties are about 10%–20% for the strongest lines ($W \gtrsim 10$ Å) and approach 50% for the weaker lines. FWHM uncertainties are generally below 20%–30%, with the level of uncertainty depending on the S/N of the composites as well as line blending (e.g., Si IV λ1398) in some cases. All measurements were carried out after Fe II$_{UV}$ and continuum subtraction, except that these corrections were not applied to Mg II λ2800.

The Fe II$_{UV}$ template covering the 1000–2000 Å region (where the most interesting lines are) was created with spectra for I Zw 1 (see Marziani et al. 1996; M03 for details). The template was intensity scaled and broadened in order to best match the observed Fe II pattern in the composite spectra. The results are summarized in the last row of Table 2. Figure 3 illustrates the deblending results for two particularly important groups of lines: Lyα + N V λ1240, and Al III λ1860 + Si III] λ1892 + C III] λ1909. The first blend is important because N V λ1240 is the only high-ionization line that shows no significant Baldwin effect (Sulentic et al. 2000a; see also § 4.5). The importance of the second blend involves the fact that the intensity ratio Si III] λ1892/C III λ1909 may be sensitive to density (n_e) and/or may be affected by metallicity trends along E1 (M01; § 4.3). We carried out a deblending procedure by assuming a Lorentzian profile for both lines in the blend and allowing for different component intensities and FWHM. A possible contamination by Fe III blends may contribute to some extent to the relatively poor fit of these lines in the A3 bin.

We consider several interesting results that can be summarized as follows:

1. O VI λ1034, Lyα, C IV λ1549, C III λ1909, and Mg II λ2800 show a systematic increase in EW as one proceeds from extreme population A (bin A3) toward the B bins. The most dramatic change is actually seen in Mg II λ2800, C IV λ1549, and also O VI λ1034, where bin-averaged EWs increase by almost a factor of 4 (a factor $\sim$10 is seen in C IV λ1549 if individual sources are considered). While we adopted a C IV centroid shift at FWHM as an E1 parameter, other C IV measures follow the E1 sequence as well.

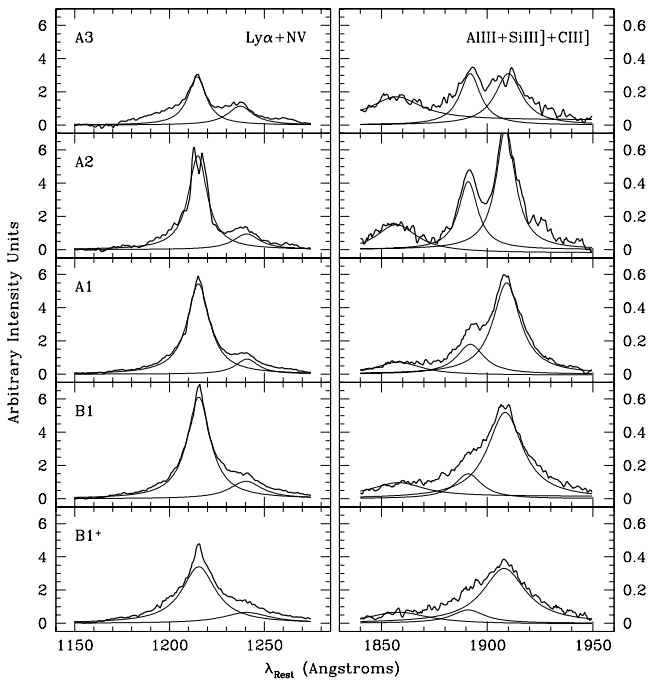

FIG. 3.—Decomposition of blended lines for the spectral types considered in this paper. *Left*: Lyα + N V λ1240. *Right*: Al III λ1860, Si III] λ1892, and C III λ1909. To all blends we subtracted in advance the underlying continuum and an Fe II$_{UV}$ emission template; Fe II$_{UV}$ emission, however, is weak around Lyα and C III λ1909. Thick lines show the profiles we fitted; thin lines show individual line contributions (assumed to have Lorentzian profiles) to the blend. No narrow component is subtracted prior to the fitting in any of the lines. While the N V λ1240 EW remains approximately constant, the Si III] λ1892/C III λ1909 intensity ratio decreases monotonically along the sequence of spectral types. Horizontal scale is rest-frame wavelength in Å; vertical scale is intensity in arbitrary units.

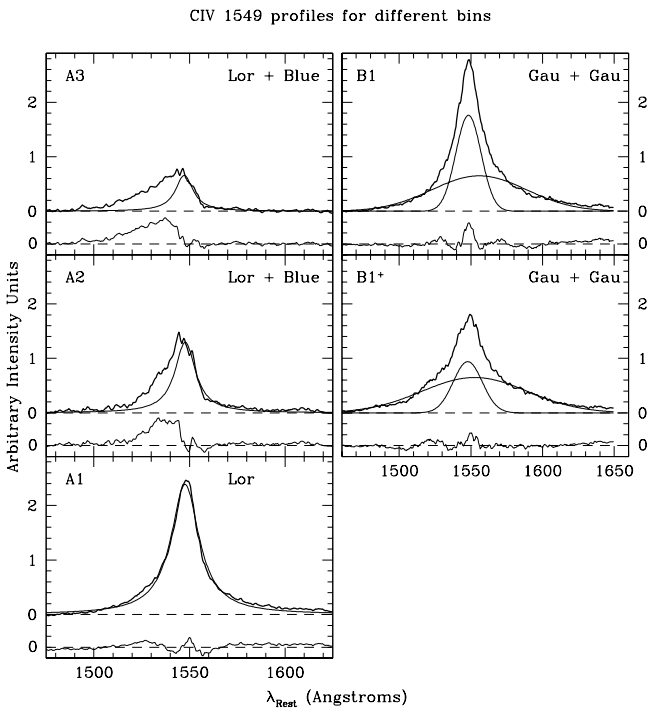

FIG. 4.—C IV λ1549 line profile decomposition for the spectral types considered in this paper. The fitted data are shown by thick lines; they are obtained from the continuum and Fe II$_{UV}$–subtracted spectra after He II λ1640, O III] λ1663, and N IV] λ1486 removal. For bin A3 and A2, the thin line superposed to the data shows the best fit provided by an unshifted Lorentzian line to the C IV λ1549 red wing. The residual is a broad and blueshifted feature, possibly associated with outflows. For bin A1, a symmetric Lorentzian provides a satisfactory fit. For spectral types B1 and B1+, two Gaussian profiles, similar to the one used by Sulentic et al. in Paper I to fit Hβ_{BC}, provide a satisfactory fit to the C IV λ1549 broad component. Narrow central residuals seen in A1 and B bins can possibly be associated with the contribution of the NLR.

2. Contrary to the above lines, N V λ1240 shows almost constant EW ($\approx$20–25 Å) across the E1 sequence. Other lines show no clear trends within measurement uncertainties.

3. The Si III] λ1892/C III λ1909 intensity ratio decreases monotonically by a factor of 4 as one proceeds from bin A3 to B1$^+$ (from 0.8 to 0.2). See § 4 for possible explanations.

4. We find a clear positive trend between FWHM and ionization potential (χ) for the principal broad lines. The correlation coefficients are in the range 0.6–0.8. FWHM typically scales linearly with χ up to $\chi \lesssim 50$ eV and saturates beyond that value. The scatter in this relation appears to be smaller for A bins. B bins suggest that some LIL such as Mg II λ2800 and Lyα deviate from the relationship with larger than expected values of FWHM. The linear part of the relation can be roughly described by the following expression: FWHM $= V_0 + \alpha\chi$, where $\alpha \sim 60-80$ and V_0 from 1000 to 3000 km s^{-1} from bin A3 to B1$^+$. The saturation occurs at about 4000 km s^{-1} for A bins and at about 5000–6000 km s^{-1} for B bins.

3.2. C IV λ1549 *Profile Decomposition*

The C IV λ1549 line deserves special attention as the best studied, and easiest to study, HIL. The C IV λ1549 intensity and relative lack of contamination by satellite lines motivated its selection as the representative HIL in the E1 parameter space. Profile centroid shift at FWHM intensity was chosen as one of the most important E1 parameters (Sulentic et al. 2000c). The blueshifted component of the C IV λ1549 line seems to disappear in sources with FWHM H$\beta_{BC} \geq 4000$ km s^{-1}, providing further support for the population A-B distinction. This fact and other previous works make it clear that both HIL and LIL cannot be treated as single-component lines. A large part of the confusion in past broad-line studies stems from this fact. The simplest possible decomposition of our composite C IV λ1549 profiles was attempted after the following processing steps. (1) The continuum was subtracted by fitting a low-order Lagrange polynomial over the region 1000–2000 Å. (2) A broadened and scaled Fe II$_{UV}$ template was subtracted (§ 3.1; Table 2). Fe II$_{UV}$ emission is not strong in any of the bin composites; however, a reasonable correspondence between the optical and UV Fe II emission strengths can be traced in the sense that bin A3 shows the strongest Fe II$_{UV}$ emission. (3) Contaminating lines near C IV λ1549, N IV] λ1486, and blended He II λ1640 + O III] λ1663 were fitted with Lorentzians and subtracted from the C IV λ1549 wings. (4) A narrow component was subtracted from the C IV λ1549 profile (see below).

Results of the C IV λ1549 decomposition are given in Figure 4 and Table 3. Results from modeling our Hβ_{BC} composites (Paper I) are useful here. We identified three reasonably unambiguous Hβ components in the context of E1 and the population A-B hypothesis. These identifications, and the adopted profile fits, are largely empirical at this stage. We focus on bins A2/A3 and B1 as representative of the two AGN populations or E1 parameter space extrema. Bin A1 is likely a mix of both population A and B sources (or a transition between the two).

1. Narrow-line region

a) Hβ. We often see an inflection between the broad-line region (BLR) and narrow-line region (NLR) components of LIL Hβ, making profile decomposition less ambiguous (Marziani et al. 1996). Bins A2/A3 show evidence for weak Hβ_{NC} emission (EW $\simeq$ 3 Å) in residuals after modeling the broad-line components (Paper I). A more significant NLR component is found in the majority of population B sources $\langle$EW$\rangle \simeq 5-6$ Å with a large scatter). If we assume a fixed ratio for Hβ_{NC}/[O III] λ5007, then the Table 1 averages for EW([O III] λ5007) imply a very weak Hβ_{NC} contribution in bins A2/A3. This ratio is about

TABLE 3
C IV λ1549 COMPONENTS

	Component 1				Component 2			
Bin	Type	λ	FWHM	Strength (%)	Type	λ	FWHM	Strength (%)
A3.....	Lorentzian	1547.3	2220	50	Blue	1532	4800	50
A2.....	Lorentzian	1547.8	2600	76	Blue	1534	3900	24
A1.....	Lorentzian	1547.7	3580	100	...	...	...	...
B1.....	Gaussian	1548.3	4170	42	Gaussian	1555.8	15590	58
B1$^+$.....	Gaussian	1547.8	4780	28	Gaussian	1552.6	17480	72

0.11 for population B sources, which would imply EW($H\beta_{NC}$) $\simeq$1 Å for bins A2/A3, which is lower than what we actually subtracted except in the "blue outlier" sources where [O III] λ5007 is extremely weak and blueshifted (Zamanov et al. 2002).

b) C IV λ1549. In our opinion it is clear that a narrow C IV $\lambda1549_{NC}$ component exists in many, especially population B, sources because we can see a profile inflection (Sulentic & Marziani 1999). The situation for C IV λ1549 is more ambiguous than for $H\beta_{BC}$ because of the lower intrinsic resolution (and often S/N) of the C IV λ1549 spectra, which less often show the inflection that can guide a profile decomposition. Either Gaussian or Lorentzian fits to the broad C IV λ1549 profiles of bin A1, B1, and $B1^+$ composites show a narrow residual. Although one cannot be sure that it is from an NLR component, that is the simplest interpretation and is empirically justified by many cases in which NLR emission is unambiguously observed. New evidence for an NLR component in, at least, population B RL quasars is given in § 4.4. We therefore argue that an uncertain NLR subtraction is better than no subtraction for the A1 and B bins. No NLR component was subtracted from bins A2/A3. The NLR profile width was assumed FWHM $\lesssim$ 2000 km s^{-1} (taking into account the fact that C IV λ1549 is a doublet). Photoionization models suggest EW(C IV $\lambda1549_{NC}$) $\simeq$ 0.1 EW([O III] λ5007) as a reasonable estimate (i.e., about 2–4 Å, using the EW([O III] λ5007) values from Table 1 and Paper I). We should point out that this EW ratio is rather similar to the flux ratio of the lines, since the continuum shape does not seem to change significantly along the E1 bins (Fig. 1). Without intercalibration of optical and UV fluxes, as well as knowledge of the NLR extinction properties (e.g., Netzer & Laor 1993), such numbers are only indicative. See Sulentic & Marziani (1999) for more quantitative estimates of the effect of a C IV λ1549 NLR component on measures of FWHM and line shift. Our adopted estimates of EW(C IV $\lambda1549_{NC}$)/EW(C IV $\lambda1549_{BC}$) show a large scatter (0.0–0.5) among individual sources in A1 and B bins.

2. Broad-line region

a) Hβ. This is the defining broad-line component for type 1 AGNs. The population A-B distinction is currently defined in terms of sources with FWHM $H\beta_{BC}$ smaller or larger than 4000 km s^{-1}. Population A2/A3 bin composites are best fitted by an unshifted Lorentzian function (Véron-Cetty et al. 2001), while for population B bins a Gaussian model works better. While the bin composite profiles are unshifted, individual sources can show red- or blueshifts of up to 4000 km s^{-1}. Profile shifts larger than about 600 km s^{-1} are seen only in population B sources (Sulentic et al. 2000a, 2000c). Double-peaked profiles are also sometimes ($\leq$5%) seen in bins $B1^+$ and $B1^{++}$.[8] Measures of FWHM $H\beta_{BC}$ can be strongly influenced by the NLR component (e.g., L/L_{Edd} and black hole [BH] mass over- and underestimated, respectively).

b) C IV λ1549. A strongly blueshifted line or line component is seen only in population A sources. The red half of the bin A2/A3 composite profiles can be reasonably well fitted with an unshifted Lorentzian model whose strength is inferred from the amount of flux redward of the adopted source rest frame. In this context extreme A3 sources should have only a weak unshifted component, with the bulk of the line flux strongly blueshifted. We do not know if this decomposition has any physical meaning, i.e., whether we have two distinct line-emitting regions or a single region producing a complex profile. There are two admittedly empirical reasons to favor the two-component model:

i) $H\beta_{BC}$ is best fitted with an unshifted Lorentzian, and there is no a priori physical reason why some HIL emission could not be produced in the clouds responsible for the LIL emission. Current models do not rule out the possibility of significant C IV emission from the LIL clouds (Korista et al. 1997), although the accurate quantitative predictions require extensive knowledge of the physical conditions there. The derived width of the best-fit C IV λ1549 Lorentzian components are in good agreement with those estimated for $H\beta_{BC}$ (about 2500 km s^{-1}; see Paper I).

ii) The fits in Figure 4 are consistent with a systematically increasing unshifted component as one proceeds from bin A3 to B1. The blueshifted (bulk of the emission in bins A2/A3) would be strongly blue asymmetric and would truncate rather sharply near the rest-frame velocity, an interesting challenge for physical models. This truncation is actually seen in sources such as I Zw 1 and Ton 28, where a single-component model is more appropriate (Sulentic et al. 2000c, 2001). We cannot distinguish between a Gaussian or Lorentzian model for the population B BLR. The choice will affect our estimate of the strength of the underlying very broad line region (VBLR). Results from $H\beta_{BC}$ fits lead us to favor, by analogy, a two-Gaussian model for C IV λ1549 population A sources involving unshifted BLR plus redshifted VBLR components. At this point we cannot place much physical meaning on these Lorentzian versus Gaussian fits; they simply reflect the relative sharpness of the line peak and the extent of the profile wings.

3. Very broad line region

a) Hβ. There is no consensus on whether or not the VBLR is a distinct component (e.g., Corbin 1997; Snedden & Gaskel 2004; Korista & Goad 2004). Only population B sources appear to show this "red shelf" or component that we model as a separate VBLR (see references in Sulentic et al. 2000a). We prefer to speak of the VBLR as a distinct component for at least two reasons: (1) we often see an inflection between the red wing of the best-fit BLR Gaussian and the red feature, and (2) we have identified sources that only show a VBLR component (Sulentic et al. 2000b). Paper I composites suggest that the best current description of the components involve (i) a BLR with zero mean shift and FWHM $\sim$5000–6000 km s^{-1}, as well as (ii) a VBLR with a mean redshift of about 5000 km s^{-1} and FWHM $\simeq$ 10,000 km s^{-1}.

b) C IV λ1549. No evidence for a significant VBLR component is seen in population A bins paralleling the results for $H\beta_{BC}$. A double-Gaussian decomposition is consistent with both BLR and VBLR C IV λ1549 components in population B bins.[9] FWHM of the components are in rough agreement with those for Hβ. Interestingly, C IV λ1549 VBLR line shifts appear to be lower ($\sim$1000 km s^{-1}) than those modeled in the $H\beta_{BC}$ composites; however, this may be a result of the fact that the two-component fitting is not necessarily a unique operation.

Furthermore, line shift values derived for such an ultrabroad component must be considered very uncertain, especially given the low S/N of many *HST* spectra.

While we currently separate population A and B sources at FWHM($H\beta_{BC}$) = 4000 km s^{-1}, if the distinction has any meaning, then it will likely involve a complex combination of parameters. There are two possible interpretations of the population A-B concept: (1) two distinct AGN populations with different central source geometry and kinematics involving

[8] Bin $B1^{++}$ was defined in Paper I for sources with $R_{Fe\,II} < 0.5$ and 8000 km s^{-1} $\lesssim$ FWHM($H\beta_{BC}$) $\lesssim$ 12,000 km s^{-1}.

[9] Although we fitted the A1 profile with a single Lorentzian, we cannot rule out the possibility that (some) A1 sources have both, a weak VBLR and a weak blueshifted (wind) component, which, along with a central unshifted component, mimic a single Lorentzian.

perhaps a critical Eddington ratio, or (2) a single main sequence involving the majority of AGNs and driven by a gradual change in the ionization parameter/Eddington ratio (see M01). The elbow shape of the source occupation in the optical plane of E1 is an argument in favor of the former interpretation (i.e., it is not a monotonic correlation). In any case, the shape suggests that bin A1 will likely blend the parameter space properties of population A and B sources. Figure 4 and Tables 1 and 2 support that view. A few sources in bin A1 (e.g., NGC 1566 and Mrk 493) show very strong NLR emission, while others show little or none. Our C IV λ1549 profile analysis supports the population A-B idea in the sense that we find C IV λ1549 line components unique to each (population A, blueshifted BLR; population B, redshifted VBLR) but mutually exclusive.

Our results appear to be robust for sources with $z < 0.8$. Richards et al. (2002) created similar C IV λ1549 composite spectra using part of the much larger and higher mean redshift ($\langle z \rangle \simeq 1.8$) SDSS quasar sample. Their spectral resolution is similar to our own, but the S/N of individual spectra are usually much lower. They binned spectra showing C IV λ1549 into four groups (each involving almost 200 sources) based on the centroid shift of C IV λ1549. We lack LIL data that would allow us to assign unambiguous population A and B tags to these bins, but the two extreme groups (Richards et al. composite D, most blueshifted; composite A, least shifted) should more or less correspond to our A2/A3 and B1/B2 samples, respectively. If this statement is true, then E1 predicts that the SDSS composite A sample should contain many RL sources and composite D should contain very few. We also note that SDSS composite A is more sharply peaked than composite D, consistent with a stronger NLR component. We applied our profile decomposition procedure to the SDSS A and D composites, kindly provided by G. Richards, and the results quantitatively verify the previous statement about their similarity to our lower redshift composites. The profiles are also consistent with the presence of a growing (from D to A) unshifted BLR component that further supports our two-component fits to the bin A2/A3 composites. Richards et al. (2002) interpret the overall shift of C IV λ1549 as the result of "missing" flux on the red side of the profile. We think that the body of evidence, within the E1 context, does not support this interpretation; e.g., the blue wing of C IV λ1549 in extreme population A sources does not resemble the blue wing of C IV λ1549 in the broader population B sources. Similarly, the blue wing on SDSS composite D is steeper than that for composite A. If we relate missing flux to obscuration, then it would be surprising to find the strongest soft X-ray emission from sources with the most extreme blueshifted C IV λ1549 profiles, since both should hardly be related.

SDSS composites cannot be used to help us decide whether there is a continuous main sequence in E1 or two distinct populations. Caution is needed in interpreting the SDSS binning because we do not know what the SDSS bin definition means in an E1 context, especially when Mg II λ2800 (wings) may be strongly affected by Fe II emission. If Mg II λ2800 follows the line shift behavior of $H\beta_{BC}$, large relative shifts C IV λ1549–Mg II λ2800 can occur in population A because of C IV λ1549 blueshifts and in population B because of possible Mg II λ2800 redshifts. If C IV λ1549 blueshifts (relative to the rest frame and not Mg II λ2800) remain a population A phenomenon at high redshift, then the SDSS results suggest that the fraction of population A sources is larger at high redshift (75% vs. our estimate that 60% of quasars are population A; Marziani et al. 2003b). This would be consistent with our suggestion that population A sources represent the "seed" population of young quasars in the universe (Sulentic et al. 2000a; Mathur 2000; Constantin & Shields 2003).

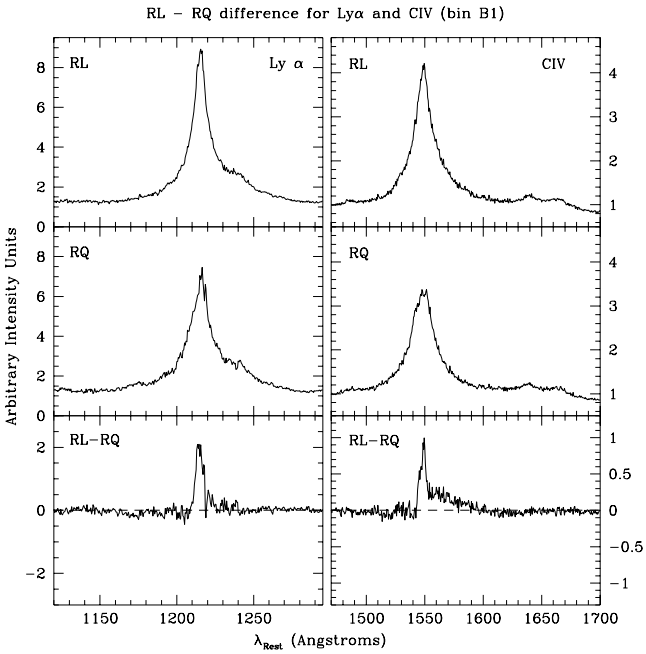

FIG. 5.—Lyα (*left*) and C IV λ1549 profiles (*right*) for RL (*top*) and RQ (*middle*) quasars. Note that, unlike in Fig. 3, contaminating lines have not been removed. Residuals (*bottom*) show that the main difference is due to a stronger narrow component in RL sources. Horizontal scale is rest-frame wavelength in Å; vertical scale is in arbitrary intensity units.

3.3. *RL-RQ Differences and Luminosity Effects*

We can also compare RL versus RQ properties using suitably constructed composites. Selection of RQ and RL subsamples from a single bin will ensure that we compare quasars with similar physical and observational properties. An extreme comparison of population A versus B will not be possible using a single bin. We would have to compare an extreme population A bin with an extreme population B one. Instead this will be a comparison between RL sources and RQ sources with optical spectra indistinguishable from them. This comparison offers hope to isolate subtle effects that might be direct manifestations of RL activity. We must use a B bin for this comparison because that is where most RL sources are found. We choose B1, which is the most densely populated and where RL and RQ objects are almost evenly represented. Radio (6 cm) and optical *V*-band fluxes were derived from data in the VCV01 catalog. A radio index (Kellermann et al. 1989) R_K was computed, and all sources with $\log(R_K) > 2$ are considered RL (see Sulentic et al. 2003). Figure 5 shows the RL and RQ composites, as well as RL-RQ residuals, for both Lyα and C IV λ1549. We see evidence for differences: (1) most significantly, stronger (EW ~ 5 Å) NLR emission in the RL sources, and (2) a possible excess redshifted BLR (or VBLR) emission in RL sources (this is also present in the Figs. 7*a*–7*d* composite difference of Richards et al. 2002). The former is not a surprise (see, e.g., Xu et al. 1999), while the latter, if real, may be an important clue. Since we know that some bin B1 RQ sources also show NLR emission, result 1 reflects a lower limit for the mean NLR contribution in bin B1 RL sources. A comparison also shows that the RL sources from this bin have, on average, stronger [O III] and $H\beta_{NC}$

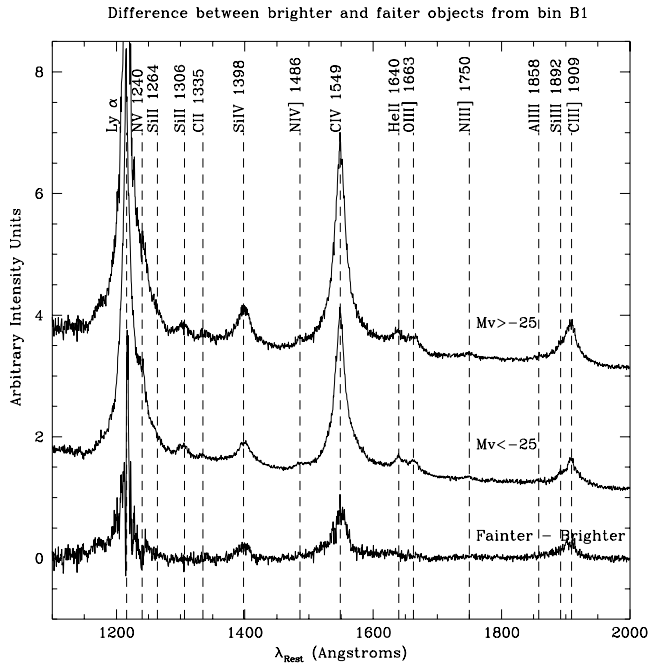

FIG. 6.—Similar division as the one shown in Fig. 5 is presented here; this time we show the difference between the fainter objects and the brighter objects from bin B1. The separation value of the absolute V-band luminosity, $M_V = -25$, is chosen in order to create two equally represented groups. The Baldwin effect (anticorrelation of the EW of a line with the luminosity is apparent for lines such as Lyα, Si IV λ1398, C IV λ1549, and Si III] λ1892, but not for lines such as N V λ1240 and Si II] λ1306). The situation is unclear for He II λ1640, O III] λ1663, and other lines because of their lower contrast.

components (typically by about 30%) than the RQ sources. There is no doubt that RQ sources exist with VBLR components as strong as the strongest observed among the RL sources (e.g., Sulentic et al. 2000b), so further tests of the red residual are needed.

In order to explore any luminosity correlation with composite spectra, we again restrict ourselves to bin B1. Sources were separated into brighter and fainter groups using $M_V = -25$ as the reference value. This value separates the bin B1 sample into two approximately even groups. Composite spectra (covering 1000–2000 Å) and differences are shown in Figure 6. One can see a difference in the broad components of all the strongest high-ionization lines (Lyα, C IV λ1549, Si IV λ1398, and C III λ1909) in the sense that the EW is larger for the lower luminosity composite spectrum (the Baldwin effect? see § 4.5 for a thorough discussion). This difference was not seen in the RL versus RQ comparison. Fainter, lower ionization lines do not show any difference; furthermore, they are weak enough that any difference would likely be undetectable.

4. DISCUSSION

4.1. *The Relevance of the Median Composites*

The use of composite spectra raises an immediate question. Do median composites yield typical quasar spectra for each bin? For example, is a symmetric profile in a median composite the result of equal numbers of blue and red asymmetric profiles? A visual inspection of our sample spectra shows, e.g., for B bins, about 60% of sources with a more or less symmetric C IV λ1549 profile, while the remainder show 10%, 20%, and 10% respectively red, blue, and indeterminate (because of low S/N) asymmetries. This suggests that median composites represent the most typical quasar spectrum and that the changes between our spectral bins are real. If our bin populations had $\gtrsim$100 objects, then we would use weighted average composites, but medians appear to be a reasonable approach at this time. It is also important to point out that bin sizes were chosen to include sources that are statistically similar within the average parameter measurement errors.

Another important question is whether or not an ensemble of line profiles with a wide distribution of widths, strengths, and asymmetries will yield a representative profile of the same type after combination. We see that many of the lines (especially the strongest) are better fitted by a Lorentzian, whatever that means physically. Is it possible, for instance, that an ensemble of Gaussian profiles will generate a Lorentzian-like shape in composite spectra, or the converse? This might lead to incorrect interpretation, and hence modeling, of line-forming regions. In order to test this possibility, we ran a simulation by combining together about 100 artificial line profiles with a wide (normal) distribution of widths and intensities, resembling the real situation to some extent. We performed the simulation with both Gaussian and Lorentzian profiles, creating median and average composites from the individual pseudospectra. The results suggest that profile type is preserved; i.e., a composite of Gaussians or Lorentzians will preserve their respective profile forms in a composite spectrum.

4.2. *Inferences From* C IV *Profile Decomposition*

Proper decomposition of emission lines in composite spectra along the E1 sequence offers insights into changes in BLR geometry and kinematics. Several results from this and previous papers provide interesting clues.

Asymmetric blueshifted HIL emission is seen almost exclusively in population A sources. In the most extreme cases a blueshift is also observed in the unusually weak [O III] λ5007 features (Zamanov et al. 2002; Marziani et al. 2003c). One simple interpretation that immediately suggests itself involves some kind of outflow from an optically thick emitting region into an optically thin NLR. In a scenario in which the broad lines arise from an accretion disk, this could involve a high-ionization disk outflow or wind. It would be strongest in population A sources and would gradually weaken or even disappear as one proceeds along the E1 sequence toward population B. Along the same sequence, an unshifted/symmetric Lorentzian HIL component (which may be analogous to the dominant LIL component) may be growing, in exactly the opposite sense of the blueshifted feature. In fact, some theoretical models predict Lorentz-like profile wings (e.g., Penston et al. 1990; Dumont & Collin-Souffrin 1990). The profile may become more Gaussian in the population B region. We have argued in a pre-E1 context that HIL versus LIL line shifts appeared to be completely uncorrelated for RQ sources and marginally correlated for the RL minority (Marziani et al. 1996). Composite spectra, binned in an E1 context, suggest that C IV and H$\beta_{\rm BC}$ may show analogous emission components except for the blueshifted HIL feature, seen only in population A, that are almost always RQ AGNs.

A very broad and redshifted VBLR component is only seen in population B sources and may be present in both HIL and LIL. Since NLR-BLR-VBLR inflections are rarely seen, there may be less spatial/kinematic decoupling between these regions for C IV than is seen for H$\beta_{\rm BC}$, where clear inflections are common. That is far from proven, because we also see LIL profiles with little or no inflection between components. Inflections may be driven by kinematics and/or orientation. There are some indications that the region producing C IV

$\lambda 1549_{\rm NC}$ emission is closer to the center than the region producing H$\beta_{\rm NC}$ (Sulentic & Marziani 1999). The C IV λ1549 VBLR may be most simply interpreted as arising at the inner edge of the classical BLR in analogy to H$\beta_{\rm BC}$ VBLR (Marziani et al. 1993; Sulentic et al. 2000b). The lower redshift of the C IV λ1549 population B source VBLR may also indicate that a high-ionization wind is still present in the VLBR, since the C IV λ1549 component is still blueshifted with respect to the corresponding Hβ component.

4.3. *BLR Structure and Kinematics*

So far there is no single picture capable of explaining the overall properties of the broad-line–emitting region. Currently fashionable models involving line-emitting clouds near an optically thick accretion disk suffer a number of difficulties. If the motions of the clouds are *Keplerian*, then they will collide with the disk and will likely be destroyed on short timescales. If one adopts an outflow/inflow model, then the entire profile will show large red- or blueshifts, because the standard, optically thick disk will obscure emission from the far side of a flow, while in reality large shifts in line profiles are rare.

Alternatively, emission lines originating from a geometrically thin, optically thick disk (e.g., Dumont & Collin-Souffrin 1990) will show extremely small FWHM when observed face-on. This situation may be relevant for population A sources, but recent work suggests that the situation is different for RL and, by analogy, other population B sources. The most jet-aligned superluminal RL sources, which should have negligible disk rotation contribution to LIL FWHM, show FWHM $\simeq$ 3000–4000 km s^{-1} (Rokaki et al. 2003; Sulentic et al. 2003). It is, however, true that core-dominated (CD) and superluminal sources with $i \rightarrow 0^{\circ}$ show systematically narrower profiles than other (FR II) RL AGNs (Sulentic et al. 2003). CD sources are displaced toward lower FWHM(H$\beta_{\rm BC}$) in the optical E1 plane, which is consistent with orientation predictions. However, even these near pole-on sources lie well above many RQ sources with similar $R_{\rm Fe\,II}$; i.e., they have larger FWHM(H$\beta_{\rm BC}$) for the same $R_{\rm Fe\,II}$ (Sulentic et al. 2003). The results for RL sources suggest that we need a considerable velocity dispersion in the vertical direction to account for observed LIL widths [FWHM(H$\beta_{\rm BC}$) $\approx$ 3000 km s^{-1}].

The above results might be telling us that the bulk of line emission in RL and population B RQ sources does not arise from a standard, optically thick accretion disk, especially when we observe FWHM LIL/HIL $\sim$ 3–4000 km s^{-1} in sources reasonably interpreted as almost disk face-on. One candidate for the line-emitting region involves the outer self-gravitating part of the disk (Collin & Huré 2001; Bian & Zhao 2002). The disk is expected to become gravitationally unstable at some radius $R_{\rm SG}$, where it will break up into rings or discrete self-gravitating clouds. The vertical velocity dispersion of such clouds may be amplified by cloud-cloud encounters. Some studies suggest that the disk can become self-gravitating at a distance from the central black hole as small as $100R_G$–$200R_G$, where R_G is the Schwarzschild radius (see, for instance, Collin & Huré 2001). A detailed theory for a self-gravitating disk is not yet available; however, it is expected that the radius of the self-gravitating region will depend on the central black hole mass and Eddington ratio (and two related and very important parameters: viscosity, α, and disk opacity). There is no consensus on the correct dependence of $R_{\rm SG}$ on parameters such as $M_{\rm BH}$ or Eddington ratio $\dot{m} = L/L_{\rm Edd}$ (here we assume that the accretion efficiency (η) does not change with luminosity; otherwise, $\dot{m} = \dot{M}/\dot{M}_{\rm Edd}$, where $\dot{M}_{\rm Edd} = L_{\rm Edd}/(\eta c^2)$).

A very simple approach for exploring this idea involves application of the Toomre stability criterion to a standard Shakura-Sunyaev disk (Shakura & Sunyaev 1973). This will give an estimate of the radius in which the stability parameter (Q) becomes approximately 1. Different models of the self-gravitating region often predict different $R_{\rm SG}$ dependence on the accretion parameters because of different initial assumptions about the outer regions of the disk (i.e., opacity, pressure, etc.). Bian & Zhao (2002) obtain in a recent work $R_{\rm SG} \propto \dot{m}^{-0.49} M_{\rm BH}^{-1.16}$ based on standard accretion disk solutions assuming dominant Kramers opacity. They assume that it is equal to the radius of the BLR $R_{\rm BLR}$ (here and below, $R_{\rm SG}$ is expressed in R_G). Collin & Huré (2001) adopt a numerical approach with realistic opacities and get a complex $R_{\rm SG}$ dependence roughly approximated by $R_{\rm SG} \propto \dot{m}^{0.16} M_{\rm BH}^{-0.46}$ for the region $\log(M_{\rm BH}) = 7$–9, $\dot{m} = 0.01$–1. Following these authors, for a BH mass $M = 10^7\ M_{\odot}$ and Eddington ratio $\simeq$1, $R_{\rm SG} \approx 10000R_G$, while for $M = 10^9\ M_{\odot}$ and $\dot{m} \simeq 0.01$, $R_{\rm SG}$ is less than about $500R_G$.

On the other hand, we can consider "superluminal" RL sources with the narrowest RL line profiles: FWHM(H$\beta_{\rm BC}$) $\lesssim$ 3000 km s^{-1}, and the narrowest population A sources, with FWHM(H$\beta_{\rm BC}$) $\lesssim$ 1000 km s^{-1}, also likely to be observed at $i \approx 0^{\circ}$. Assuming orbital motion with Keplerian angular velocity ($\Omega_{\rm K}$), one can write for these apparently face-on sources:

$$\mathrm{FWHM} \simeq \Delta v \simeq \nu \Omega_{\rm K} R_{\rm SG}, \qquad (1)$$

where Δv is the vertical velocity dispersion, assumed to be proportional to the *Keplerian* velocity by a factor of ν. A reasonable guess for ν is about 0.1–0.2. One can easily show that FWHM of 3000 km s^{-1} implies a radius of about $5000R_G$, while 1000 km s^{-1} implies $500R_G$, values quite close to the size of the self-gravitating region assumed above. Even if the agreement is perhaps fortuitous and the exact $R_{\rm SG}$ dependence is far from certain, it is reasonable to conclude that $R_{\rm SG}$ ($\sim R_{\rm BLR}$) may be smaller in population B sources by a factor $\sim$10 and that this may leave a very "small" emitting surface for any standard optically thick, geometrically thin disk component. Part of the line profile may be produced in the disk if it is illuminated by a geometrically thick inner region or by disk warping (e.g., Bachev 1999) and if it is not extremely hot (which would completely ionize the lower ionization species). On the other hand, the presence of a blueshifted component can be most simply explained as the signature of an outflow from an optically thick disk. The disk-wind scenario can produce blueshifted high-ionization lines, as already suggested in several works (e.g., Murray & Chiang 1997; Bottorff et al. 1997). If our interpretation is correct, this implies that the wind strength increases toward the most extreme population A sources (bins A2/A3 with the strongest $R_{\rm Fe\,II}$). Population B sources may have a much lower, or may not develop, a wind component. Following these considerations, we propose a simple BLR scenario (see also Fig. 1 in Collin & Huré 2001):

1. A "hot" innermost accretion region, located inside some transition radius ($R_{\rm Tr} \lesssim 50R_G$–$100R_G$). Our data leave the structure of this region open to speculation, although we may reasonably assume that the continuum region (or part of a geometrically thick, optically thin advection-dominated accretion flow (ADAF; see Narayan et al. 1998 for an exhaustive review) can heat the outer line-emitting region.

2. An optically thick, geometrically thin disk whose extent decreases by a factor $\sim$10 from population A to population B.

The heated disk produces a wind that is responsible for the blueshifted C IV λ1549 component. The outer region of the disk may emit H$\beta_{\rm BC}$ and other LILs as well in population A sources. The disk may become almost negligible in population B sources because $R_{\rm SG}$ may become as small as $100R_G$–$200R_G$ (e.g., Bachev & Strigachev 2004).

3. A self-gravitating and fragmented zone where line emission might arise in dense gas clumps. This region may be the *entire BLR* for population B sources, while it may contribute mainly to LIL emission in population A objects.

Within the context of this model + E1, we can eventually explain several observational results from this paper as well as from previous works:

1. The different vertical velocity dispersion in the self-gravitating zone for population B (closer) and population A (farther) sources accounts for different line widths at $i \rightarrow 0^{\circ}$.

2. After subtraction of an unshifted/symmetric Lorentzian component, the blueshifted residual shows reasonable persistency in shape: the intensity may change but not the overall shape. The blue component becomes marginal at bin A1. This behavior is consistent with the idea that the blue component comes from a disk-generated wind, where the kinematics (velocity field) is strongly affected by the detailed properties (e.g., magnetic field structure and terminal wind velocity). The overall shape of a line arising in a disk wind will be less dependent on the radial distance where the wind originates. In other words, our model provides an easy explanation why population A sources tend to show decoupled HIL-LIL components, while population B sources show more similar C IV λ1549 and H$\beta_{\rm BC}$ profiles. In the most extreme cases, there are sources where the entire C IV λ1549 profile resembles the blue component alone (e.g., I Zw 1, Ton 28; Sulentic et al. 2000c).

Leighly (2004) presented an interesting explanation of the apparent anticorrelation between the strengths of the central and the blueshifted (wind) components. The wind that gives rise to the blueshifted component might filter the EUV ionizing radiation that would otherwise reach the outer, self-gravitating parts (where the unshifted line component might originates). The wind cannot, however, filter effectively the hard X-rays that are reprocessed in LIL emission in the same region.

An alternative approach is to ascribe the entire profile of C IV in A2/A3 bins to an outflow (wind). In such a case, the redward emission is seen either because the disk is (partially) transparent to C IV photons or because of higher inclinations, resulting in significant projection of the Keplerian/radial component of the wind velocity onto the line of sight. Both possibilities seem somewhat unlikely, at least for these extreme bins.

3. There are trends between χ and FWHM (e.g., Tytler & Fan 1992). Population A sources can be explained with a split BLR: inner HIL-emitting regions and an outer LIL-emitting region. Since we expect that gas motion will retain its circular velocity in the wind and will acquire an upward and outward velocity component, the velocity dispersion in the wind will be higher than for a Keplerian velocity component in the disk. LIL emission from the outer, fragmented region will therefore be narrower. In population B sources we expect a "normal" BLR stratification: HIL emitted closer to the central continuum source than LIL. In general, we expect that both HIL and LIL will be emitted rather close to the central continuum source, accounting for the rather high ionization spectrum. This outline requires testing with photoionization models.

Reverberation mapping indicates continuum response times of C III λ1909 consistent with that of H$\beta_{\rm BC}$ (at least in NGC 5548; Clavel et al. 1991). This result suggests that C III λ1909 is primarily produced in the low ionization–emitting part of the BLR. Under the assumption of nearly constant [Si/C] abundance ratio, the behavior of the Si III] λ1892/C III λ1909 intensity ratio along the E1 sequence can then be understood in terms of increasing electron density toward type A3 (M01) in the LIL-emitting BLR. The critical n_e of the C III λ1909 line is $\sim 10^{9.5}$ cm^{-3}, much lower than that of the Si III] λ1892 line, $\sim 10^{11}$ cm^{-3}. Therefore, for $n_e \gtrsim 10^{10}$ cm^{-3}, the C III λ1909 line should be more and more collisionally suppressed with increasing n_e, while the Si III] λ1892 line should become favored. We also observe a consistent increase in the strength of the Al III λ1860 line, with the intensity ratio Al III λ1860/C III λ1909 reaching $\sim$0.8 for spectral type A3 ($n_e \sim 10^{11}$ cm^{-3}). The Al III λ1860 line is expected to strengthen with increasing electron density (Baldwin et al. 1996; Korista et al. 1997). However, as pointed out by the referee, chemical abundance may not be constant along the E1 sequence. We do not have information on the [Si/C] and [Al/C] abundance ratios. Intensity ratios involving nitrogen lines suggest that supersolar metallicity is appropriate for extreme population A (i.e., A3) sources. From Table 2, we have N V λ1240/C IV λ1549 $\approx$ 1 and N V λ1240/He II λ1640 $\approx$ 3 for A3, while for A1 N V λ1240/C IV λ1549 $\approx$ 0.25, and N V λ1240/He II λ1640 $\approx$ 1.5. It is intriguing that we are observing again, for spectral type A3, line ratios that are more frequently found in high-z quasars (Hamann & Ferland 1999). Highly supersolar nitrogen enrichment may have been produced by star formation with a top-loaded initial mass function (Hamann & Ferland 1992; § 4.5). It is possible that changes of line ratios from population B to population A and along the A spectral type are due to *both* an n_e increase and a metallicity increase. Quantifying these effects is a challenge for further work.

4.4. *Radio-loud Sources: Black Hole Spin and Host Morphology?*

Comparison of RL and RQ line profiles (§ 3.2) in the E1 context should begin with a comparison of population A and B sources. The differences that we find between population A and B HIL C IV composites are even larger than for LIL H$\beta_{\rm BC}$. We can say with some confidence that sources showing low EW, blueshifted, and blue asymmetric C IV λ1549 have low probability ($P < 1\%$) to be RL. Population B sources have a reasonably high probability to be RL ($P \sim 50\%$; Marziani et al. 2003b). Since not all population B sources are RL, we focus (§ 3.3) on a particular bin (B1) within population B where we can compare C IV λ1549 properties for RQ and RL AGNs that appear to be spectroscopically indistinguishable. Our RL-RQ difference spectrum is shown in Figure 5. We see evidence for a significantly stronger NLR component in population B RL sources. This might be explained if a significant part of the narrow-line emission is produced in interactions between a radio jet and the ambient medium, forming presumably a narrow-line–bright cocoon around the jet (e.g., Steffen et al. 1997; Axon et al. 1998). Aside from a possible excess of redshifted broad-line gas in the RL sources, population A RL and RQ line profiles look very similar, as was also found for H$\beta_{\rm BC}$ (Marziani et al. 2003b). The VBLR component, which might be related to this redshifted gas, is seen in both RL and RQ population B AGNs (Sulentic et al. 2000b) and therefore is not a RL signature. One is tempted to consider host galaxy morphology as a major

difference between the RL and RQ sources in bin B1. RL sources tend to be hosted in elliptical galaxies (Pagani et al. 2003), while a typical population B RQ source involves a classical Seyfert 1 such as NGC 5548, hosted in a spiral. Perhaps the population B emission-line spectrum indicates that RL activity is possible as far as physical conditions near the BH are concerned, but host morphology dictates whether it happens or not. If it were that simple, however, we might expect to see many frustrated RL sources involving trapped core emission (unless it is self-quenching under that circumstance).

The bin B1 results emphasize the fact that population B RQ and RL sources are spectroscopically indistinguishable as far as *broad* lines are concerned. This may be telling us that radio loudness is not directly dependent on, or strongly influencing, BLR structure (and therefore the structure of the accretion disk, at least at $r \gtrsim 100R_G$). This makes a circumstantial case for the role of black hole spin, which is unlikely to have any influence on the accretion disk structure outside $10R_G$–$100R_G$, where the UV line emission likely originates, at least if the Bardeen-Petterson effect (Bardeen & Petterson 1975) is not in play. The black hole spin can, however, play a significant role in jet production (e.g., Blandford & Znajek 1977). The fact that the majority of RL sources occupy B bins may be associated with a change of the innermost accretion disk structure (from a thin disk to an ADAF? see Ròzanska & Czerny 2000 and references therein) that is probably triggered by the lower accretion rate (or by some function of the black hole mass and the accretion rate). If true, the accretion disk structure change (from thin disk to ADAF) will be a necessary but not sufficient condition for radio loudness (i.e., the ultimate trigger will be the black hole spin, subject to the environmental caveat mentioned above). In this scenario only B bin objects that contain a rapidly spinning black hole would be able to produce powerful jets.

4.5. *A Local "Baldwin Effect" Driven by the Eddington Ratio?*[10]

Measurement of broad-line EWs reveals both a trend and the lack of a trend (see also § 3.1):

1. Lyα, C IV λ1549, Mg II λ2800, and O VI λ1034 show a systematic EW decrease by factors of 2–4 as one proceeds from bin B1$^+$ to A3. Table 2 shows the same trend for other lines, but caution is needed when interpreting blended lines and data for lines with EW $\lesssim$ 5 Å that have estimated uncertainties $\gtrsim$30% at the 1 σ confidence level.
2. The N V λ1240 line shows no trend with EW(N V λ1240) $\approx$ 20–25 Å in all spectral bins.

These results essentially describe the so-called Baldwin effect (hereafter BE; originally defined as an anticorrelation between rest-frame EW C IV λ1549 and source luminosity at 1450 Å: Baldwin 1977). It is well known that N V λ1240 does not follow the BE trend (see Sulentic et al. 2000a for references before 1999; Dietrich et al. 2002; Green et al. 2001; Croom et al. 2002). While the original BE showed a tight correlation involving a few tens of sources, more recent work (Dietrich et al. 2002; Warner et al. 2003) shows it to be a very loose correlation that only becomes significant over a wide range in continuum luminosity $\log(\lambda L_\lambda) = 42$–$48$ ergs s^{-1} (e.g., Kinney et al. 1990). Considering the large dispersion, it is not surprising that several studies using small samples found no evidence for a BE (see Sulentic et al. 2000a for numerical simulations and a thorough discussion of the issue).

The BE-like trend found between our spectral bins does *not* represent a dependence on luminosity. The E1 sequence is independent of source luminosity (Sulentic et al. 2000c) and is more likely governed by the Eddington ratio (M01; Marziani et al. 2003b). In fact, population B spectral bins contain more high-luminosity sources than population A because RL in our sample are overluminous, and overrepresented, relative to RQ sources (see also Boroson & Green 1992). Our BE trend is also *not* BH mass-dependent (e.g., Warner et al. 2003): the largest BH masses are again found in population B (M03). If we compare the average $\dot{m}$ values for our bins (from M03) with EW(C IV λ1549) measures from our composite spectra, we obtain the following approximate relation: $\log \mathrm{EW(C\ IV\ }\lambda1549) \simeq 1.35 - 0.67 \log(L/M)$ excluding bin B1$^+$. Our models predict that B1$^+$ sources are simply more inclined B1 sources (M01). Including B1$^+$ yields $\log \mathrm{EW(C\ IV\ }\lambda1549) \simeq 3.22 - 0.39 \log(L/M)$, using L/M bin averages from M03, or $\log \mathrm{EW(C\ IV\ }\lambda1549) \simeq 3.54 - 0.47 \log(L/M)$, if bin averages are taken from this paper (L/M is measured in solar units). If we consider all sources (RQ and RL), a robust fitting method yields $\log \mathrm{EW(C\ IV\ }\lambda1549) \simeq 3.23 - 0.36 \log(L/M)$, which becomes $\log \mathrm{EW(C\ IV\ }\lambda1549) \simeq 3.40 - 0.41 \log(L/M)$ for RQ sources alone.

Parameter dispersion in the Baldwin effect [from EW(C IV λ1549) $\approx$ 20–200 Å] is well reproduced by sources spanning the range $\sim$0.02–1 in $\dot{m}$ regardless of the fitting solution details. Highest $\dot{m}$ sources show the lowest EW(C IV λ1549), and it is a well-established fact that NL Seyfert 1 galaxies show the lowest EW(C IV λ1549) (Marziani et al. 1996; Rogriguez-Pascual et al. 1997; Sulentic et al. 2000a) and are likely to radiate close to the Eddington limit. Many known NL Seyfert 1 galaxies are relatively low redshift/luminosity sources that tend to blur standard BE correlations at the low-luminosity end (see, e.g., Brotherton & Francis 1999) because they show EW(C IV λ1549) similar to the high-redshift quasars (Sulentic et al. 2000a). Sulentic et al. (2000a) suggested that the BE might be caused by preferential (probably driven by selection effects and/or intrinsic evolution) detection of large $\dot{m}$ sources at high redshift. In a flux-limited sample, in which L and z are highly correlated, an "evolutionary" (redshift-dependent) Baldwin effect is expected and is indeed found in the Large Bright Quasar Survey (Green et al. 2001). Given a sample that is complete in terms of $\dot{m}$, the BE may survive with even larger scatter or disappear depending on the relative importance of evolutionary and selection effects (see Dietrich et al. 2002). Deeper surveys may detect larger EW(C IV λ1549) sources at high redshift: see, for example, the distribution of EW(C IV λ1549) at $z \gtrsim 4$ in Constantin et al. (2002). Intriguingly, they detect several sources with EW(C IV λ1549) $\gtrsim$ 50 Å at $\log L \approx 46.5$ ergs s^{-1}.

Interpretation of the BE has been highly controversial, with suggestions encompassing orientation effects (Netzer 1985), selection effects (Sulentic et al. 2000a and references therein), black hole mass (Wandel 1999; Warner et al. 2003), and Eddington ratio (Sulentic et al. 2000a; Shang et al. 2003; Baskin & Laor 2004). A continuum softening with increasing luminosity (Wandel 1999) is a less model-dependent explanation. Warner et al. (2003) suggest that the driving parameter may be the central black hole mass. These authors computed the BH mass using a modified Kaspi et al. (2000) relation, employing FWHM C IV λ1549 instead of FWHM Hβ and assuming virial motions. This *does not demonstrate* that mass is driving the BE because it is assumed to be $M \propto L^{0.7}$, and this assumption

[10] We call the L/L_{Edd}-dependent Baldwin effect a "local" Baldwin effect also, since it is defined through low-z, low to moderate luminosity quasars and Seyfert 1 nuclei, in opposition to the canonical Baldwin effect, which emerges considering high-z, high-luminosity quasars.

makes the computation in part circular. Furthermore, we question the validity of estimating BH masses using C IV λ1549 (e.g., Vestergaard 2002; Warner et al. 2003, 2004). While Hβ_{BC} shows average broad-line profiles that can be argued to arise in virialized clouds, C IV λ1549 is blue asymmetric and blueshifted in about 60% of the sources. In many cases, the shift is significant, and in some virtually all of the line flux is displaced to the blue side of the local rest frame. It is not at all clear that the clouds (or wind?) producing the HIL emission can be assumed to be virialized. Finally, failure to correct for NLR emission in the C IV profile will contribute to the dispersion in BH mass that might be present. NLR emission tends to decrease the dispersion BLR FWHM measures (FWHM measures for population B become more like population A). Figure 5 shows that NLR-uncorrected FWHM C IV measures will underestimate BH mass and overestimate L/L_{Edd} values for RL sources.

Our work shows that a C IV $\lambda1549_{NC}$ exists in, at least, population B sources and that a significant part (if not all) of C IV λ1549 emission in bins A2/A3 arises in a wind. The terminal wind velocity could be only indirectly related to Keplerian (i.e., virialized) motions. The overall velocity dispersion is even less likely to be related to virial motion in near face-on sources, where the accretion disk likely obscures the receding part of the flow. The C IV λ1549 line profile in such cases is almost fully blueshifted with respect to the rest frame. While any correlation with mass will be little affected over several orders of magnitude (Warner et al. 2003), any more fundamental correlation with $\dot{m}$ may be entirely washed out (the $\dot{m}$ range is a factor $\lesssim$50; Woo & Urry 2002). Comparing FWHM Hβ and C IV in different spectral bins (population B with and without C IV $\lambda1549_{NC}$ subtraction) suggests that errors could be at least a factor $\sim$10 for some objects (since, for example, the FWHM ratio C IV λ1549 Hβ is $\approx$3 in I Zw 1; Marziani et al. 1996, 2003b). However, a shallow trend between EW(C IV λ1549) and L/L_{Edd} is noted in a large sample of quasars of redshift $0 \lesssim z \lesssim 5$ (Warner et al. 2004), which seems to support our results for $z \lesssim 0.8$.

Another circumstantial element supporting a role for the accretion rate $\dot{m}$ in the BE involves the constancy of EW(N V λ1240) and the increasing intensity ratio N V λ1240/C IV λ1549 along the sequence from B1$^+$ to A3. The large values of EW(N V λ1240) for all spectral types are suggestive of solar or supersolar metallicity (Turner et al. 2003; Bentz & Osmer 2004). It is not unreasonable to suppose that N may have been enhanced by vigorous formation of massive stars that burn H via the CNO cycle in the AGN circumnuclear regions. The largest enrichment may have occurred in relatively young or rejuvenated quasars radiating at large accretion rates as NL Seyfert 1 galaxies are thought to be (several NL Seyfert 1 galaxies hosts may be merging dwarf or barred galaxies; Krongold et al. 2001; Crenshaw et al. 2003).

5. CONCLUSIONS

We computed and analyzed composite UV spectra for five different spectral bins along the main sequence of the E1 optical parameter plane. Data were analyzed following Paper I, which considered similar composite spectra for the optical region involving Hβ, our representative LIL. We measured the FWHM and EW of a number of emission lines focussing on C IV λ1549, our representative HIL. Our main results include the following:

1. We decompose HIL C IV λ1549 into possible NLR, BLR, and VBLR components, many of which have LIL analogs. We consider them to be distinct line-emitting regions. Type 2 AGNs show only NLR LIL and HIL emission. Type 1 AGNs are known with pure BLR, pure VBLR, and, most often, composite BLR+VBLR (with and without NLR) spectra if they belong to population B. A strong asymmetric blueshifted BLR HIL component is unique to population A (bins A2/A3) sources. A reasonably strong and redshifted VBLR is unique to HIL and LIL in population B (bins B1 and B1$^+$) sources.
2. We infer an n_e trend along the E1 sequence using the ratio of the semiforbidden lines Si III] λ1892 and C III λ1909. Under the assumption of a nearly constant chemical abundance along E1, we find that density increases by about an order of magnitude between bins B1$^+$ and A3. However, there are indications that both density and metallicity may increase from extreme B bins to extreme A bins.
3. We compare subsamples of RL and RQ sources in bin B1. We find an excess of NLR and redshifted broad-line emission in the RL subsample. The former represents virtual proof that NLR line emission is present in the spectra of many type 1 AGNs.
4. We advance the following empirically driven model for the structure of the accretion flow:

   a) An inner, hot, optically thin (possibly ADAF) disk, located inside $R_{Tr} \lesssim 100R_G$.

   b) A standard thin disk, between R_{Tr} and R_{SG}, producing most of the optical continuum. This is the place where a wind may originate and produce the blueshifted C IV λ1549 component.

   c) An outer self-gravitating region at $r > R_{SG}$, producing most of the broad-line emission.

R_{Tr} and R_{SG} are functions of the accretion parameters. An eventual discontinuity in their behavior as functions of M and $\dot{m}$ may account for the existence of different quasar populations (e.g., population A-B).

5. We suggest that the Eddington ratio is the primary driver of the Baldwin effect rather than source luminosity. This suggestion is motivated by the robust BE that we find in E1, which is luminosity-independent. This explains why high-redshift sources might preferentially show low EW and blueshifted C IV λ1549 if population A sources are the seed (i.e., youngest high-accreting, lowest mass BH) AGNs. This interpretation is supported by comparison of our low-redshift sample with the first results from higher redshift SDSS quasars. The latter show an increase in the fraction of sources with a blueshifted C IV λ1549 HIL: a defining characteristic of population A AGNs.

R. B. and J. W. S. acknowledge the kind hospitality and the financial support from the Osservatorio Astronomico di Padova, where much of this work has been done. We thank G. Richards for providing his SDSS composite spectra in an electronic form. We are indebted to an anonymous referee for his/her constructive criticism.

REFERENCES

Axon, D. J., Marconi, A., Capetti, A., Maccetto, F. D., Schreier, E., & Robinson, A. 1998, ApJ, 496, L75
Bachev, R. 1999, A&A, 348, 71
Bachev, R., & Strigachev, A. 2004, Astron. Nachr., 325, 317
Baldwin, J. A. 1977, ApJ, 214, 679
Baldwin, J. A., et al. 1996, ApJ, 461, 664
Bardeen, J. M., & Petterson, J. A. 1975, ApJ, 195, L65
Baskin, A., & Laor, A. 2004, MNRAS, 350, L31

Bentz, M. C., & Osmer, P. S. 2004, AJ, 127, 576
Bian, W., & Zhao, Y. 2002, A&A, 395, 465
Blandford, R. D., & Znajek, R. L. 1977, MNRAS, 179, 433
Boroson, T. A. 2002, ApJ, 565, 78
Boroson, T. A., & Green, R. F. 1992, ApJS, 80, 109
Bottorff, M., Korista, K. T., Shlosman, I., & Blandford, R. D. 1997, ApJ, 479, 200
Brotherton, M. S., & Francis, P. J. 1999, in ASP Conf. Ser. 162, Quasars and Cosmology, ed. G. Ferland & J. Baldwin (San Francisco: ASP), 395
Clavel, J., et al. 1991, ApJ, 366, 64
Collin, S., & Huré, J.-M. 2001, A&A, 372, 50
Constantin, A., & Shields, U. C. 2003, PASP, 115, 592
Constantin, A., et al. 2002, ApJ, 565, 50
Corbin, M. R. 1997, ApJ, 485, 517
Crenshaw, D. M., Kraemer, S. B., & Gabel, J. R. 2003, AJ, 126, 1690
Croom, S. M., et al. 2002, MNRAS, 337, 275
Czerny, B., Rozanska, A., & Kuraszkiewicz, J. 2004, A&A, submitted (astro-ph/0403507)
Dietrich, M., Hamann, F., Shields, J. C., Constantin, A., Vestergaard, M., Chaffee, F., Foltz, C. B., & Junkkarinen, V. T. 2002, ApJ, 581, 912
Dumont, A. M., & Collin-Souffrin, S. 1990, A&A, 229, 313
Francis, P. J., Hewett, P. C., Foltz, C. B., Chaffee, F. H., Weymann, R. J., & Morris, S. L. 1991, ApJ, 373, 465
Gammie, C. F., Shapiro, S. L., & McKinney, J. C. 2004, ApJ, 602, 312
Green, P. J., Forster, K., & Kuraszkiewicz, J. 2001, ApJ, 556, 727
Hamann, F., & Ferland, G. 1992, ApJ, 391, L53
———. 1999, ARA&A, 37, 487
Horne, K., Peterson, B. M., Collier, S. J., & Netzer, H. 2004, PASP, 116, 465
Jackson, N., & Browne, I. W. A. 1991, MNRAS, 250, 422
Janiuk, A., Życki, P. T., & Czerny, B. 2000, MNRAS, 314, 364
Kaspi, S., et al. 2000, ApJ, 533, 631
Kellermann, K. I., Sramek, R., Schmidt, M., Shaffer, D. B., & Green, R. 1989, AJ, 98, 1195
Kerber, F., & Rosa, M. 2000, ST-ECF Newsletter, 27, 4, http://www.stecf.org/newsletter/stecf-nl-27.pdf
Kinney, A. L., Rivolo, A. R., & Koratkar, A. P. 1990, ApJ, 357, 338
Komossa, S., & Meerschweinchen, J. 2000, A&A, 354, 411
Korista, K. T., Baldwin, J., Ferland, G., & Verner, D. 1997, ApJS, 108, 401
Korista, K. T., & Goad, M. R. 2004, ApJ, 606, 749
Krongold, Y., Dultzin-Hacyan, D., & Marziani, P. 2001, AJ, 121, 702
Kuraszkiewicz, J. K., Green, P. J., Crenshaw, D. M., Dunn, J., Forster, K., Vestergaard, M., & Aldcroft, T. L. 2004, ApJS, 150, 165
Leighly, K. M. 2004, ApJ, 611, 125
Maccarone, T. J., Gallo, E., & Fender, R. 2003, MNRAS, 345, L19
Marziani, P., Sulentic, J. W., Calvani, M., Perez, E., Moles, M., & Penston, M. V. 1993, ApJ, 410, 56
Marziani, P., Sulentic, J. W., Dultzin-Hacyan, D., Calvani, M., & Moles, M. 1996, ApJS, 104, 37
Marziani, P., Sulentic, J. W., Zamanov, R., Calvani, M., Dultzin-Hacyan, D., Bachev, R., & Zwitter, T. 2003a, ApJS, 145, 199 (M03)
Marziani, P., Sulentic, J. W., Zwitter, T., Dultzin-Hacyan, D., & Calvani, M. 2001, ApJ, 558, 553 (M01)
Marziani, P., Zamanov, R., Sulentic, J. W., & Calvani, M. 2003b, MNRAS, 345, 1133
Marziani, P., Zamanov, R., Sulentic, J. W., Calvani, M., & Dultzin-Hacyan, D. 2003c, Mem. Soc. Astron. Italiana, 74, 492
Mathur, S. 2000, MNRAS, 314, L17
Mirabel, I. F. 2004, Prog. Theor. Phys. Suppl., in press (astro-ph/0404156)
Murray, N., & Chiang, J. 1997, ApJ, 474, 91
Narayan, R., Mahadevan, R., & Quataert, E. 1998, in Theory of Black Hole Accretion Disks, ed. M. A. Abramowicz, G. Bjornsson, & J. E. Pringle (Cambridge: Cambridge Univ. Press), 148
Netzer, H. 1985, MNRAS, 216, 63
Netzer, H., & Laor, A. 1993, ApJ, 404, L51
Nicastro, F. 2000, ApJ, 530, L65
Pagani, C., Falomo, R., & Treves, A. 2003, ApJ, 596, 830
Penston, M. V., Croft, S., Basu, D., & Fuller, N. 1990, MNRAS, 244, 357
Peterson, B. M. 1993, PASP, 105, 247
———. 1997, An Introduction to Active Galactic Nuclei (Cambridge: Cambridge Univ. Press)
Pounds, K. A., Done, C., & Osborne, J. P. 1995, MNRAS, 277, L5
Richards, G. T., Vanden Berk, D. E., Reichard, T. A., Hall, P. B., Schneider, D. P., SubbaRao, M., Thakar, A. R., & York, D. G. 2002, AJ, 124, 1
Rodriguez-Pascual, P. M., Mas-Hesse, J. M., & Santos-Lleo, M. 1997, A&A, 327, 72
Rokaki, E., Lawrence, A., Economou, F., & Mastichiadis, A. 2003, MNRAS, 340, 1298
Ròzanska, A., & Czerny, B. 2000, A&A, 360, 1170
Schlegel, D. J., Finkbeiner, D. P., & Davis, M. 1998, ApJ, 500, 525
Schneider, D. P., et al. 2002, AJ, 123, 567
Shakura, N. I., & Sunyaev, R. A. 1973, A&A, 24, 337
Shang, Z., Wills, B. J., Robinson, E. L., Wills, D., Laor, A., Xie, B., & Yuan, J. 2003, ApJ, 586, 52
Snedden, S. A., & Gaskell, C. M. 2004, in ASP Conf. Ser. 311, AGN Physics with the Sloan Digital Sky Survey, ed. G. T. Richards & P. B. Hall (San Francisco: ASP), 197
Steffen, W., Gomez, J. L., Raga, A. C., & Williams, R. J. R. 1997, ApJ, 491, L73
Sulentic, J. W., Calvani, M., & Marziani, P. 2001, Messenger, 104, 25
Sulentic, J. W., & Marziani, P. 1999, ApJ, 518, L9
Sulentic, J. W., Marziani, P., & Dultzin-Hacyan, D. 2000a, ARA&A, 38, 521
Sulentic, J. W., Marziani, P., Zamanov, R., Bachev, R., Calvani, M., & Dultzin-Hacyan, D. 2002, ApJ, 566, L71 (Paper I)
Sulentic, J. W., Marziani, P., Zwitter, T., Dultzin-Hacyan, D., & Calvani, M. 2000b, ApJ, 545, L15
Sulentic, J. W., Stirpe, G. M., Marziani, P., Zamanov, R., Calvani, M., & Braito, V. 2004, A&A, in press (astro-ph/0405279)
Sulentic, J. W., Zamfir, S., Marziani, P., Bachev, R., Calvani, M., & Dultzin-Hacyan D. 2003, ApJ, 597, L17
Sulentic, J. W., Zwitter, T., Marziani, P., & Dultzin-Hacyan, D. 2000c, ApJ, 536, L5
Turner, T. J., et al. 2003, ApJ, 594, 128
Tytler, D., & Fan, X.-M. 1992, ApJS, 79, 1
Vanden Berk, D. E., et al. 2001, AJ, 122, 549
Véron-Cetty, M.-P., & Véron, P. 2001, A&A, 374, 92 (VCV01)
Véron-Cetty, M.-P., Véron, P., & Goncalves, A. C. 2001, A&A, 372, 730
Vestergaard, M. 2002, ApJ, 571, 733
Wandel, A. 1999, ApJ, 527, 649
Warner, C., Hamann, F., & Dietrich, M. 2003, ApJ, 596, 72
———. 2004, ApJ, 608, 136
Wills, B. J., et al. 1995, ApJ, 447, 139
Woo, J.-H., & Urry, C. M. 2002, ApJ, 579, 530
Xu, C., Livio, M., & Baum, S. 1999, AJ, 118, 1169
Zamanov, R., & Marziani, P. 2002, ApJ, 571, L77
Zamanov, R., Marziani, P., Sulentic, J. W., Calvani, M., Dultzin-Hacyan, D., & Bachev, R. 2002, ApJ, 576, L9